ECOGRAPHY

Research

Forecasting community reassembly using climate-linked spatio-temporal ecosystem models

James T. Thorson, Mayumi L. Arimitsu, Lewis A. K. Barnett, Wei Cheng, Lisa B. Eisner, Alan C. Haynie, Albert J. Hermann, Kirstin Holsman, David G. Kimmel, Michael W. Lomas, Jon Richar and Elizabeth C. Siddon

J. T. Thorson (https://orcid.org/0000-0001-7415-1010) ✉ (james.thorson@noaa.gov), Habitat and Ecological Processes Research Program, Alaska Fisheries Science Center, National Oceanic and Atmospheric Administration, Seattle, WA, USA. – M. L. Arimitsu, Seabird and Forage Fish Ecology Program, Marine Ecosystems Office, US Geological Survey, Alaska Science Center, Juneau, AK, USA. – L. Barnett (https://orcid.org/0000-0002-9381-8375), Groundfish Assessment Program, Alaska Fisheries Science Center, NOAA, NMFS, Seattle, Seattle, WA, USA. – W. Cheng and A. J. Hermann (https://orcid.org/0000-0002-0253-7464), Joint Inst. for the Study of the Atmosphere and Ocean, Univ. of Washington, Seattle, WA, USA, and Pacific Marine Environmental Laboratory, NOAA, Seattle, WA, USA. – L. B. Eisner and E. Siddon, Ecosystem Monitoring and Assessment, Alaska Fisheries Science Center, NOAA, NMFS, Juneau, AK, USA. – A. C. Haynie, Economic and Social Sciences Research, Alaska Fisheries Science Center, National Oceanic and Atmospheric Administration, Seattle, WA, USA. – K. Holsman, Status of Stocks and Multispecies Assessment, Alaska Fisheries Science Center, National Oceanic and Atmospheric Administration, Seattle, WA, USA. – D. G. Kimmel, Recruitment Process Program, Alaska Fisheries Science Center, NOAA, NMFS, Seattle, Seattle, WA, USA. – M. W. Lomas, Bigelow Laboratory for Ocean Sciences, East Boothbay, ME, USA. – J. Richar, Shellfish Assessment Program, Alaska Fisheries Science Center, NOAA, NMFS, Seattle, Seattle, WA, USA.

Ecography
44: 612–625, 2021
doi: 10.1111/ecog.05471

Subject Editor: Otso Ovaskainen
Editor-in-Chief: Miguel Araújo
Accepted 13 December 2020

Ecosystems are increasingly impacted by human activities, altering linkages among physical and biological components. Spatial community reassembly occurs when these human impacts modify the spatial overlap between system components, and there is need for practical tools to forecast spatial community reassembly at landscape scales using monitoring data. To illustrate a new approach, we extend a generalization of empirical orthogonal function (EOF) analysis, which involves a spatio-temporal ecosystem model that approximates coupled physical, biological and human dynamics. We then demonstrate its application to five trophic levels for the eastern Bering Sea by fitting to multiple, spatially unbalanced datasets measuring physical characteristics (temperature measurements and climate-linked forecasts), primary producers (spring and fall size-fractionated chlorophyll-a), secondary producers (copepods), juveniles (age-0 walleye pollock), adult consumers (five commercially important fishes), human activities (seasonal fishing effort) and mobile predators (seabirds). We identify the spatial niche for each ecosystem component, as well as dominant modes of variability that are highly correlated with a known bottom–up driver of dynamics. We then measure spatial overlap between interacting variables (using Schoener's-D) and identify that age-0 pollock have decreased spatial overlap with copepods and increased overlap with adult pollock during warm years, and also that adult pollock have increased overlap with arrowtooth flounder and decreased overlap with catcher–processor fishing effort during these warm years. Given the warming conditions that are projected for the coming decade, the model forecasts increased prey and competitor overlap involving adult pollock (between age-0 pollock, adult pollock and arrowtooth flounder) and decreased overlap with the copepod forage base and with the catcher–processor fishery during future warming. We recommend that joint species distribution models be

extended to incorporate 'ecological teleconnections' (correlations between distant locations arising from known mechanisms) arising from behavioral adaptation by mobile animals as well as passive advection of nutrients and planktonic juvenile stages.

Keywords: empirical orthogonal function analysis, EOF, joint dynamic species distribution model, spatial community reassembly, vector autoregressive spatio-temporal model

Introduction

Climate change is altering productivity and structure of both terrestrial and marine ecosystems (Mora et al. 2018). Changes in ecosystem structure occur in part due to community reassembly (Schaefer et al. 2008) wherein spatial patterns and/or phenology shift differently for individual species (Kuczynski and Grenouillet 2018). This leads to changing spatial and phenological overlap between ecosystem components, which in turn alters facultative/competitive interactions (Ettinger and HilleRisLambers 2017) as well as the selective filters that link regional and local species pools (Kuczynski and Grenouillet 2018).

Community reassembly is also likely to affect the spatial overlap between human activities and ecosystem services, thereby intensifying geopolitical and intersectoral conflicts between beneficiaries of ecosystem services (Mora et al. 2018, Pinsky et al. 2018, Baudron et al. 2020). Understanding community reassembly is important to mitigate these conflicts, not only to identify sustainable activities and to plan conservation or management responses (Gouezo et al. 2019), but also to forecast ecological conditions and community interactions for effective dynamic and adaptive ecosystem-based management (Bonan and Doney 2018, Holsman et al. 2019).

Accurate forecasting of ecological conditions requires assimilating process research and monitoring data, and statistical fitting of these data requires methods to assimilate spatially and seasonally unbalanced sampling (Cressie et al. 2009). Forecasting spatial and temporal community reassembly requires spatial multispecies models linking elements at all ecosystem levels including physical drivers, primary and secondary producers, consumers and human impacts (Thorson et al. 2019, Hollowed et al. 2020). Given that the data available to parameterize such ecosystem models often varies in spatial and temporal extent and resolution among ecosystem components, there is need for statistical techniques that can accommodate monitoring data from multiple seasons with different temporal and spatial extents. In particular, statistical fitting of these data require methods to assimilate spatially and seasonally imbalanced observations (Cressie and Wikle 2011). Traditional data assimilation approaches for ecosystem modeling rely on relatively simple dimension–reduction methods such as principle components analysis or empirical orthogonal function (EOF) analysis (Trenberth et al. 2014). However, how best to account for imbalanced sampling within such approaches remains an open question, particularly in the context of spatio-temporal statistical models, where such EOF approaches have only recently been extended to account for spatial and temporal dependence (Thorson et al. 2020a).

Observed ecosystem responses are greatly dependent on the spatial and temporal scales at which they are analyzed and the scale of processes driving their dynamics (Levin 1992). While many ecological models assume that local population and community states are largely determined by local biotic and abiotic conditions, such local conditions are often spatially autocorrelated (Legendre 1993) and sometimes synchronous with those at geographically distant locations. For example, atmospheric and oceanic systems are driven by teleconnections (e.g. the El Niño Southern Oscillation) whereby physical mechanisms can cause simultaneous changes in local dynamics at multiple locations (Alexander et al. 2002). Synchrony among plant and animal populations also frequently arises at broad spatial scales due to fitness optimization (local populations overwhelming potential predators) and oscillations arising in stage-structured populations (Gouhier et al. 2010). Spatial synchrony in population or community dynamics is determined by spatial variation in species–environment relationships, strength of density dependence and connectivity through animal movement (Walter et al. 2017 and references therein). Migration or dispersal can cause local population states to be dependent on conditions occurring both in past seasons and at different locations, as species responses are integrated over environmental conditions encountered annually or even throughout an individual's lifetime. Therefore, ecosystem forecasting requires methods that can estimate nonlocal correlations among ecosystem components at multiple spatial extents, as well as correlations among seasons.

In the following, we demonstrate how to identify associations among ecosystem variables representing physics, primary and secondary producers, consumers, human activities and managed or protected species (Fig. 1). Importantly, we identify spatial variation in each variable, but also allow spatial patterns in one variable to be associated with the state of another variable at geographically distant locations, as well as variables measured in other seasons. By assimilating both measurements and projections of physical variables, we then forecast potential changes in overlap between predator and prey species, as well as human impacts. We conclude by outlining how future research can continue to improve our capacity to forecast multi-trophic and nonlocal dynamics.

Methods

We seek to develop a spatio-temporal ecosystem model that can measure and forecast community reassembly. Specifically, we

seek to account for nonlocal mechanistic associations between multiple system components ('ecological teleconnections') that are measured seasonally at different times throughout the year, while also forecasting these components via linkage to forecasts from an earth systems model. To do so, we expand recent developments to generalize EOF analysis using a spatio-temporal model (Thorson et al. 2020a). This generalization decomposes spatio-temporal patterns into three components:

1. Temporal variation (β) for each variable, where these intercepts are specified to follow a random-walk.
2. Spatial variation (ω) in the expected value for each variable, representing long-term spatial patterns.
3. Spatio-temporal variation (ε), estimated as one or more dominant modes of ecosystem variability as well as a map representing the spatial response for each variable to these estimated modes of variation.

The third component of this decomposition is analogous to EOF analysis, and generates time series representing modes of ecosystem variability as well as maps of ecosystem response. However, we estimate this spatio-temporal generalization to EOF after accounting for expected spatial and temporal components. This 'joint modelling framework' specifically allows for spatially and seasonally unbalanced sampling of ecosystem variables, while propagating 'predictive errors' when interpolating between sampled locations and addressing 'measurement errors' in both physical and biological variables.

Model structure

Specifically, we model the value $y(g, c, t)$ for ecosystem variables at multiple locations in several years; g indexes each of n_g modeled locations, c indexes each of n_c variables and t indexes each of n_t years (we use parentheses to indicate indexing for model variables and parameters, and subscripts to indicate variable names). Each variable is modeled using a main effect of time and space, as well as spatio-temporal variation:

$$y(g,c,t) = \underbrace{\beta_1^*(c,t) + \beta_2(c)}_{\text{Temporal main effect}} + \underbrace{\omega^*(g,c)}_{\text{Spatial main effect}} + \underbrace{\varepsilon^*(g,c,t)}_{\substack{\text{Spatio-temporal interaction} \\ \text{generalizing EOF}}}$$

This additive decomposition estimates temporal and spatial main effects in addition to the spatio-temporal EOF term, such that EOF indices only represent interannual changes in spatial overlap between ecosystem variables. This is well suited to identifying community reassembly, but future studies may modify this decomposition (e.g. eliminating the temporal main effect estimated here, such that estimated modes of variability incorporate both temporal and spatio-temporal variation). Temporal terms are specified to estimate correlated dynamics across variables; spatial and spatio-temporal components estimate a spatial correlation function representing similarities for nearby locations; and spatio-temporal components additionally include correlations among years. The temporal main effect includes two components, $\beta_1^*(c,t)$ and $\beta_2(c)$, and terms are identifiable by treating $\beta_1^*(c,t)$, $\omega^*(g, c)$ and $\varepsilon^*(g, c, t)$ as random effects. Intercept $\beta_1^*(c,t)$ follows a random-walk process for each variable with initial condition $\mu_{\beta_1}(c)$ and variance $\sigma_\beta^2(c)$, and $\beta_2(c)$ is used to approximate a compound Poisson-gamma process for biomass sampling data that includes zeros (Supporting information).

Specifically, the spatio-temporal term $\varepsilon^*(g, c, t)$ incorporates covariance among locations g, ecosystem variables c and years t. Conceptually, it represents synchronous changes in the spatial configuration of each ecosystem variable among years, and also specifies that certain variables are measuring the same underlying process:

$$\varepsilon^*(g,c,t) = \sum_{x=1}^{n_x}\sum_{f_t=1}^{n_{f_t}}\sum_{f_c=1}^{n_{f_c}} a(g,x)\lambda_t(t,f_t)\lambda_c(c,f_c)\varepsilon(x,f_c,f_t)$$

where $a(g, x)$ is the association of each location g with a spatial knot x (i.e. $\mathbf{A}$ is a sparse matrix representing bilinear interpolation between knots, where $a(g, x) = 0$ for all but three knots x for each location g), $\lambda_c(c, f_c)$ is the association between variable c and spatio-temporal factor f_c (i.e. $\mathbf{\Lambda}_c$ is the loadings matrix among variables), and $\lambda_t(t, f_t)$ associates year t with an estimated mode of spatio-temporal variability ($\mathbf{\Lambda}_t$ is the loadings matrix among years). Previous studies have used a factor-decomposition among species (Thorson et al. 2015) or among years (Thorson et al. 2020a), but this is the first to do both simultaneously. We specifically estimate $\mathbf{\Lambda}_t$ to predict synchronous changes in spatial configuration of each ecosystem variable, and specify $\mathbf{\Lambda}_c$ a priori to intercalibrate field measurements and forecasts of physical variables. In this instance, estimated loadings matrix $\mathbf{\Lambda}_t$ then approximates the covariance among years, $\mathrm{Var}_{t|g,c}(\boldsymbol{\varepsilon}^*) = \mathbf{\Lambda}_t\mathbf{\Lambda}_t^{\mathrm{T}}$.

In the following, we incorporate both field measurements and climate-linked projections of several ecosystem components. Accounting for systematic differences between field measurements and model hindcasts is called 'delta-change methods' in earth systems models (Hay et al. 2000). We accomplish delta-change correction by modelling field-measurements and projections for a given process as two separate variables c_1 and c_2, but assuming that these variables respond similarly to spatio-temporal terms, i.e. $\lambda_c(c_1, f_c) = \lambda_c(c_2, f_c) = 1$ for the factor f_c representing this spatio-temporal variation in this ecosystem component, and $\lambda_c(c_1, f_c) = \lambda_c(c_2, f_c) = 0$ otherwise. Meanwhile, variable c_1 and c_2 have different spatial and temporal variation, i.e. such that the difference $\omega^*(g, c_1) - \omega^*(g, c_2)$ represents the disagreement between field-measurements and hindcasted values for that process at each location g. Future research could further refine this approach by incorporating further restrictions on the covariance among categories $\mathrm{Var}_{c|g,t}(\boldsymbol{\varepsilon}^*)$. For example, structural equation modelling (Kaplan 2001) would define this covariance via a set of hypothesized causal relationships, e.g. where the dependency of biological variables upon changes in specific physical variables could be estimated and used to predict future counterfactual changes (Grace and Irvine 2020).

This allows a joint model (where biological and physical variables are both treated as response variables as done here) to still support inference similar to a conventional linear model (where physical variables are treat as 'independent' and biological variables 'dependent'), although we do not pursue the topic further here.

We then fit data using either a normal distribution and identity link function, e.g. for temperature, or a Poisson-link delta-gamma distribution (Thorson 2018) for zero-inflated samples of biology (Supporting information for details and interpretation), and both involve estimating a residual variance $\sigma_b^2(c)$ as fixed effect. This Poisson-link delta-gamma model specifies a Bernoulli distribution using a complementary log–log link for encounter/non-encounters (i.e. the probability mass at zero for a delta-model), and simultaneously specifies that positive catches follow a Gamma distribution (the probability distribution for non-zeros in a delta-model), where variable $\exp(y(g, c, t))$ is defined as the expected value for this sampling process. We also specify a hyper-distribution for spatial variation at a reduced set of 'knots,' and we specifically use the computationally efficient SPDE approach (Lindgren et al. 2011) involving an estimated decorrelation rate κ and a matrix representing geometric anisotropy $\mathbf{H}$.

Estimation

We estimate all parameters using the vector autoregressive spatio-temporal (VAST) package (Thorson and Barnett 2017) in the R statistical environment (<www.r-project.org>). This software package permits alternative specifications for the spatial correlation among locations, the use of covariates affecting density (to improve predictions) or the measurement process (to intercalibrate data from multiple sampling gears), and many other choices (Thorson 2019), although we do not explore these alternative specifications in detail here. The model integrates across latent variables representing spatial variation $\omega(x, c)$ at every knot x and variable c, spatio-temporal variation $\varepsilon(x, f_c, f_t)$ for every mode of variability f_t and each modeled category f_c, and changes in intercepts $\beta_1^*(c,t)$; these latent variables are treated as random effects. The model involves estimating fixed effects, including the initial intercept for each variable $\mu_{\beta_1}(c)$ and the second intercept $\beta_2(c)$ for those variables fitted using a delta-model, as well as variance parameters including the magnitude of residual variation $\sigma_b^2(c)$ for each variable, loadings matrix among years $\mathbf{\Lambda}_t$, the variance of the random-walk variance in intercept $\sigma_\beta^2(c)$, as well as decorrelation rate κ_n and geometric anisotropy $\mathbf{H}$.

The model estimates fixed effects by identifying their values that maximize the marginal likelihood. The marginal likelihood, in turn, is calculated when integrating the joint log-likelihood across the value of random effects. This multidimensional integral is approximated by the Laplace approximation using Template Model Builder (Kristensen et al. 2016), and TMB also calculates the gradient of the approximated marginal log-likelihood which is then minimized within the R statistical environment (<www.r-project.org>). The probability of spatial variables is approximated using the stochastic partial differential equation (SPDE) approximation (Lindgren et al. 2011), and standard errors are calculated using a generalization of the delta method (Kass and Steffey 1989). For identifiability, $\lambda_t(t, f_t) = 0$ for all $f_t > t$ (i.e. $\mathbf{\Lambda}_t$ is constrained to be a lower-triangle matrix), and estimated columns of $\mathbf{\Lambda}_t$ are all orthogonal as a result of maximum-likelihood estimation. We then apply a 'PCA' rotation to $\mathbf{\Lambda}_t$ prior to presenting results (Thorson et al. 2016); this rotation specifies that the first column of the rotated matrix represents the largest portion of variance explained by $\mathbf{\Lambda}_t$, and therefore represents the 'dominant mode of variability' similar to that estimated by EOF analysis.

Ecosystem components and data compilation

Model components

We fit to twenty ecosystem variables obtained from four seasons spanning 1982–2030 in the eastern Bering Sea (Supporting information). We specifically compile seasonal records of:

1. Physical environment, including summer bottom and winter surface temperature records (Lauth and Conner 2016, Huang et al. 2017) as well as regional ocean modelling system (ROMS) hindcasts and projections under future climate scenarios (Hermann et al. 2019);
2. Primary producer concentration, in this case size-fractionated phytoplankton (0.7–10 μm and > 10 μm) during spring and fall (Eisner et al. 2016, Lomas et al. 2020);
3. Secondary producer concentration, in this case *Calanus glacialis* and *C. marshallae* copepodite stage 3 to adult concentrations ('copepod concentrations') in spring and fall (Eisner et al. 2014, Kimmel et al. 2018);
4. Abundance of age-0 pollock in near-surface waters during fall (Farley et al. 2007);
5. Bottom-associated fish and crab species that are subject to commercial fishing, sampled by bottom trawl during the summer (Lauth and Conner 2016);
6. Human activities, in this case commercial records of fishing effort from catcher–processor fleet in the winter/spring ('winter A-season') and summer/fall ('summer B-season'); and
7. Migratory bird species that overlap with human activities, in this case, seabirds during fall foraging (Drew and Piatt 2015).

Each variable is sampled at locations (latitude, longitude and vertical position above the seafloor) that vary among variables and years (Supporting information). We specifically emphasize densities and changes in spatial overlap between adult pollock, juvenile age-0 pollock that adult pollock cannibalize and arrowtooth flounder which consumes juvenile and competes with adult pollock (Supporting information for ecological relationships among variables). We also interpret overlap between age-0 pollock and fall copepod concentrations, adult pollock and the fall catcher–processor fleet, as well as the fall catcher–processor fleet and seabirds (shearwaters). The region had high interannual variability in regional temperature from 1982 to 1999, followed by warm and cold 'stanzas' representing lower-frequency fluctuations in temperature.

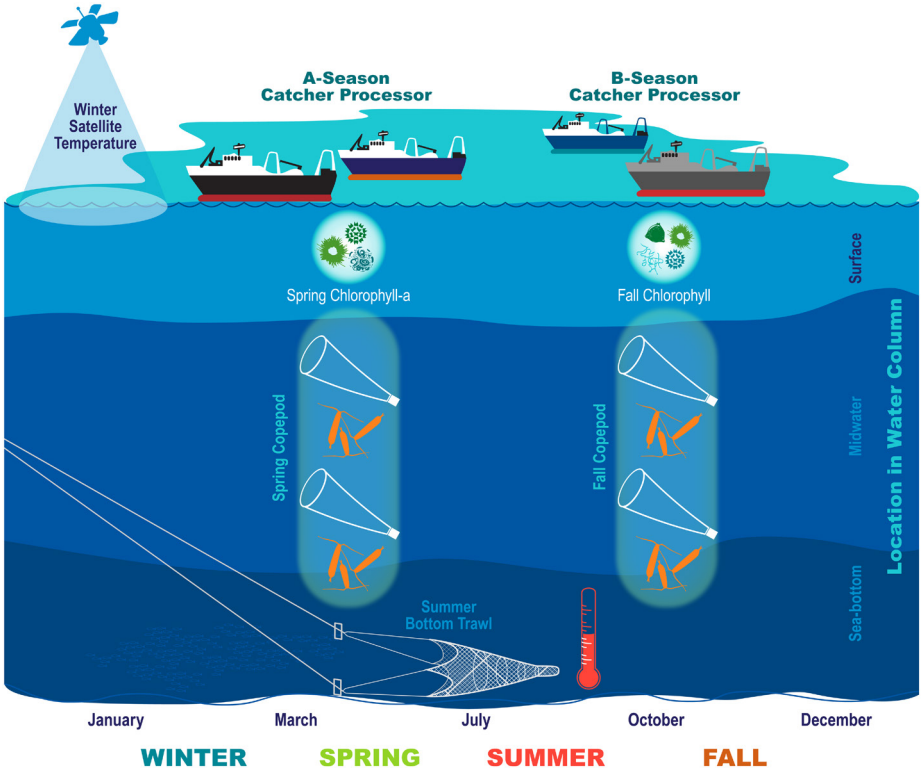

Figure 1. Visualization of seasonal timing (horizontal axis, from winter on the left to fall on the right) and vertical availability of data (vertical axis, from seafloor on bottom to surface at top) of physical and biological variables (see Supporting information for full list).

Model specification and interpretation

We specify that summer bottom temperature has the same spatio-temporal variation for both net-sensor measurements and ROMS hindcasts/projections, and the same for winter surface temperature for the NOAA reanalysis product and ROMS hindcasts/projections. We estimate spatial and spatio-temporal variation at 100 knots, and project from these knots to 8000 extrapolation cells (a.k.a. quadrature points) when calculating derived quantities; knots are distributed in proportion to the 8000 extrapolation-grid cells, and we confirm that results are similar when specifying fewer knots. We include two modes of spatio-temporal variation ($n_{f_t} = 2$) and focus upon the rotation of the loadings matrix $\mathbf{\Lambda}_t$, where the first column $\boldsymbol{\lambda}_t$ of this rotated matrix represents the dominant mode of spatial variability in the ecosystem. We specifically compare this dominant mode of variability with the spatial extent of near-bottom waters less than or equal to 2°C (termed 'cold pool extent'); previous process research suggests that cold-pool extent is a major organizing principle for ecosystem function in the eastern Bering Sea (Sigler et al. 2016). We include only two modes because some modeled years (e.g. 2020–2030) only have two measured variables, and estimating additional columns of $\mathbf{\Lambda}_t$ would not be identifiable given the current model structure. This assumption could be relaxed in future studies by imposing a distribution on the temporal dynamics of $\mathbf{\Lambda}_t$, e.g. specifying a hyperdistribution for $\lambda_t(f, t)$ given its value in the previous year $\lambda_t(f, t-1)$. However, we have avoided this for clarity of presentation in this case-study demonstration, and recommend it as a topic for future development and exploration. Including two modes (rather than a single mode) allows for changes in spatial overlap that are more complicated than can be explained purely via a single time-series indicator. Future studies could additionally interpret the 2nd mode (rather than just the first as we do here); this has done by past studies (Thorson et al. 2020a), although we avoid the topic here for clarity of presentation.

We also compute the spatial overlap between select ecosystem components, where overlap is defined using Schoener's-D (Schoener 1970, Carroll et al. 2019) as calculated at each of 8000 extrapolation points that are uniformly distributed throughout the modeled area. We interpret changes in spatial overlap as driving a likely change in the strength of ecological linkages between components, and therefore as indicating community re-assembly under projected climate conditions.

Model validation

Finally, we provide a self-test simulation experiment to confirm that parameters are identifiable and that confidence intervals have an appropriate width. In particular, we conduct 50 simulation replicates. In each simulation replicate we:

1. Simulate new sampling data (at the same location and time for each variable) conditional upon estimated fixed effects and predicted random effect values;
2. Refit the estimation model to simulated data and record the loadings matrix $\mathbf{\Lambda}_t$ that replicate;

3. Apply the same PCA rotation, and then reorder columns such that the first column is maximally correlated with the dominant axis of variability from the original fit;
4. Compare the 'true' dominant mode of variability $\boldsymbol{\lambda}_t$ (as estimated from the original fit to real data) with $\boldsymbol{\lambda}_t$ estimated in each simulation replicate, specifically by calculating the correlation.

For a well-performing model, the distribution of $\boldsymbol{\lambda}_t$ estimates will be distributed around the original value and will fall approximately within the originally estimated confidence intervals.

Results

The spatio-temporal model estimates large differences in average spatial distribution for physics measurements and forecasts, phytoplankton and meso-zooplankton, fish/decapod densities, fishing effort and seabird components of the ecosystem (Fig. 2). For example, small and large size-fraction chlorophyll concentrations are highest in spring near Zhemchug Canyon in the northern Bering Slope while fall large size-fraction chlorophyll concentrations are higher near the Pribilof Islands and inshore near Nunivak Island

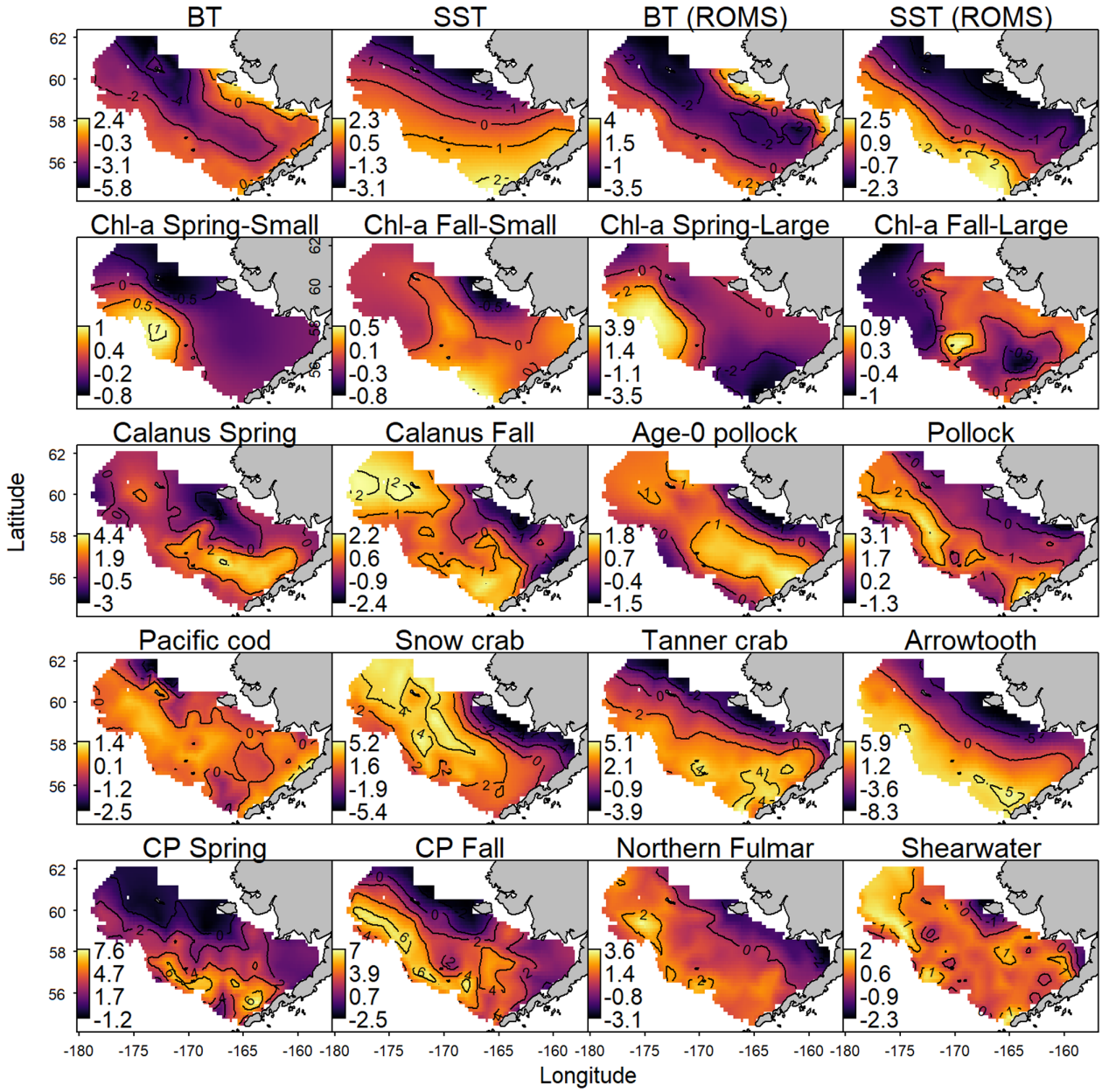

Figure 2. Spatial variation in the value of each variable included in the model (ω_g), representing variation between locations in the long-term average value. The difference between bottom temperature (BT) and surface temperature (SST) measurements and associated ROMS forecasts (ROMS_BT and ROMS_SST) represents differences in the average measurement relative to ROMS predictions, which is analogous to a delta-correction method for intercalibrating these two data sources.

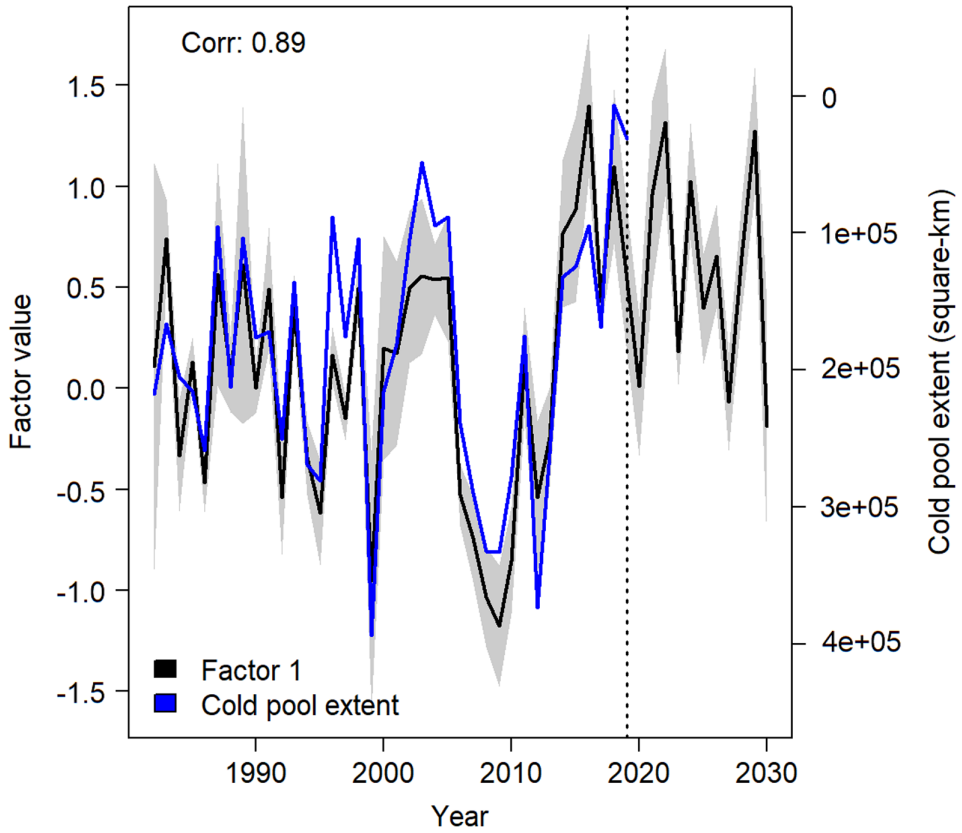

Figure 3. Dominant mode of ecosystem variability for spatio-temporal variation (black lines ± one standard error, left y-axis scale) and cold-pool extent (blue line, right y-axis scale), while listing the Pearson correlation (top-left corner), while indicating the year (2019) separating physical hindcasts and projections (vertical dotted line).

and the Kuskokwim River delta. The model estimates highest copepod concentrations over the middle shelf in spring with increased abundance over the outer shelf and the north Bering Sea in fall. Similarly, average distribution for demersal fish and crustacean species is highly species-specific, with highest densities for pollock and cod in the middle domain, for tanner crab in the southern portion, and snow crab in the northern portion; juvenile (age-0) pollock have higher concentration to the south of adult pollock. The catcher–processor fleet in the winter A-season has a more southern distribution of fishing effort than during the summer B-season. Average distributions of seabirds were also distinct between species: northern fulmars are most abundant along the outer shelf while high densities of shearwaters are persistent along the inner shelf near Bristol Bay.

The model then estimates the dominant mode of variability in spatial distribution for each ecosystem component after controlling for these differences in average spatial distribution. The dominant mode of variability 1982–2018 is highly correlated with the spatial extent of cold near-bottom waters as measured during bottom trawling (Fig. 3). Spatial responses to this mode of variability vary widely among ecosystem components (Fig. 4); in some cases, these patterns are well recognized while others have received less attention. For well-studied examples, pollock and cod show elevated densities in the northern portion near St. Matthew Island in years with a smaller-than-average cold-pool, and arrowtooth flounder shows elevated densities throughout the middle domain in these same years. Concentrations of small and large chlorophyll increase in the middle shelf in spring and near Zhemchug Canyon in fall, while spring copepod densities increase and fall copepod densities decrease near Bristol Bay in the southern middle domain. The winter A-season fishery shows elevated effort near Bristol Bay while the summer B-season shows elevated effort throughout the middle domain. Finally, shearwaters are clustered in the central and southern portions of the study area, especially along the inner shelf near Bristol Bay.

This dominant mode of variability is then projected over the coming decade (2020–2030) by using information in the ROMS hindcast/projection variables (Fig. 5, showing evenly spaced years); it projects that the ecosystem is likely to remain similar to warm conditions over the coming decade (2020–2030). Based on these predicted conditions, the model projects increased densities of arrowtooth flounder throughout the middle domain in 2029, a northward shift in pollock, and elevated summer B-season fishing effort in the middle domain relative to patterns in earlier years, 1983/1994/2006 (i.e. comparing bottom with higher rows in Fig. 5).

These patterns paint a clear picture for how bottom–up environmental conditions have driven shifts in spatial overlap

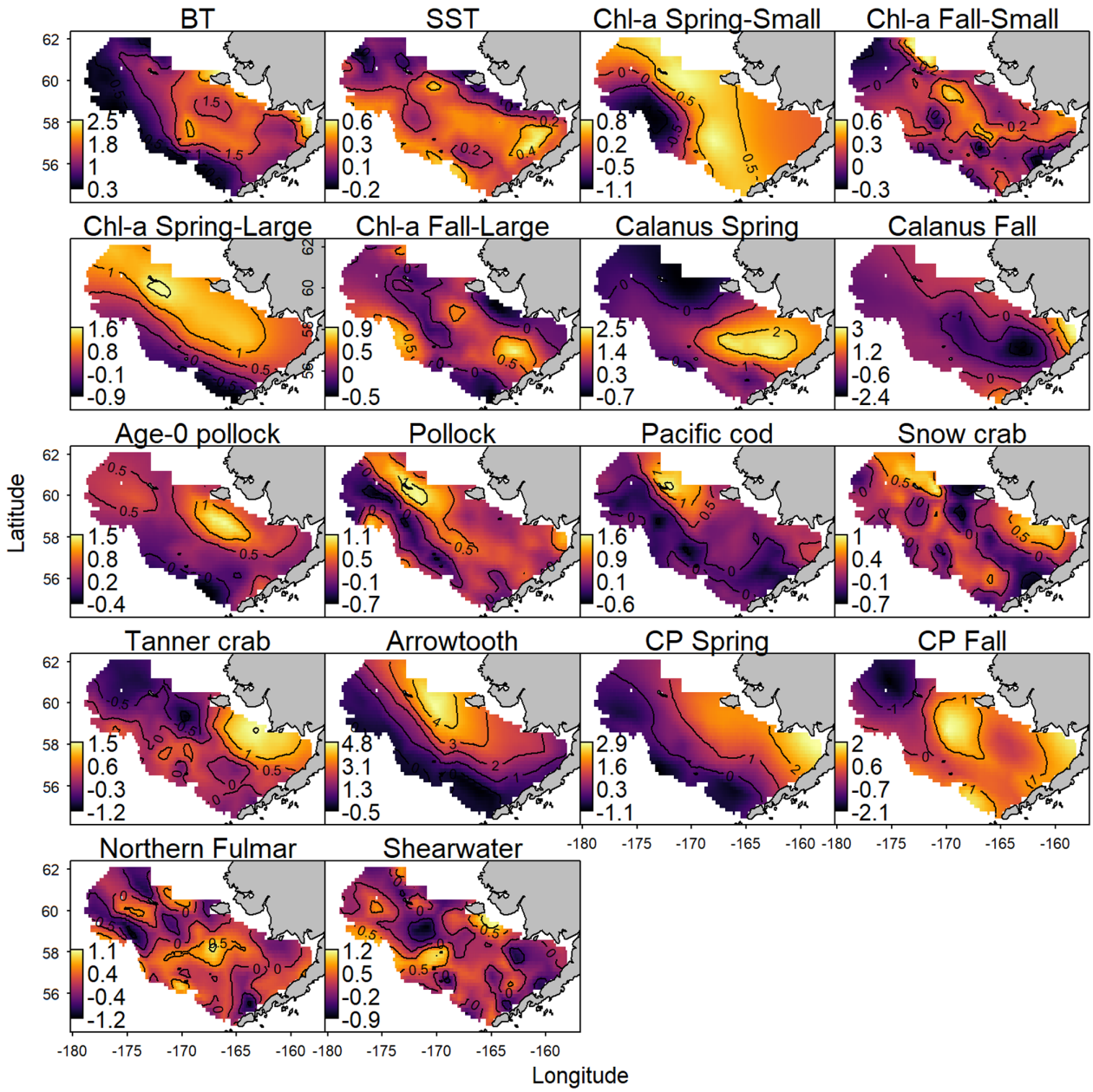

Figure 4. Spatial response for each variable to a positive value of the primary mode of ecosystem variability (shown in Fig. 3); see color legend in bottom-left side of each panel. Variation for biological variables is modeled in log-space, such that a value of 0.1 at location s indicates that a year t when index $\lambda_{\varepsilon}'(t,1)=1$ is expected to have a 10% increase for that variable at that location. Variation for physical variables is modeled in natural space, such that a value of 0.1 at location s indicates a 0.1 increase for that location when $\lambda_{\varepsilon}'(t,1)=1$.

between prey, predators and human activities. We illustrate shifts in overlap between pollock and other system components (Fig. 6); a warm stanza (1999–2005) was associated with elevated overlap with arrowtooth flounder and decreased overlap with B-season fishing effort. This was followed by a cold stanza (2006–2013) with larger cold-pool extent, during which walleye pollock showed decreased overlap with arrowtooth flounder and increased overlap with B-season fishing effort. The subsequent warm stanza (2014–2019) again showed opposite patterns which are expected to continue into the future (2020–2023), resulting in greater overlap with an important predator (arrowtooth flounder) and lower overlap with human impacts (fishing effort).

Finally, the self-test simulation experiment confirms that the model is able to accurately reconstruct the 'true' dominant mode of variability when data are simulated conditional upon estimated fixed-effect and predicted random-effect values (Fig. 7). Specifically, the correlation between original and re-estimated values for the dominant mode of variability is high (average correlation = 0.95), and above 0.75 in

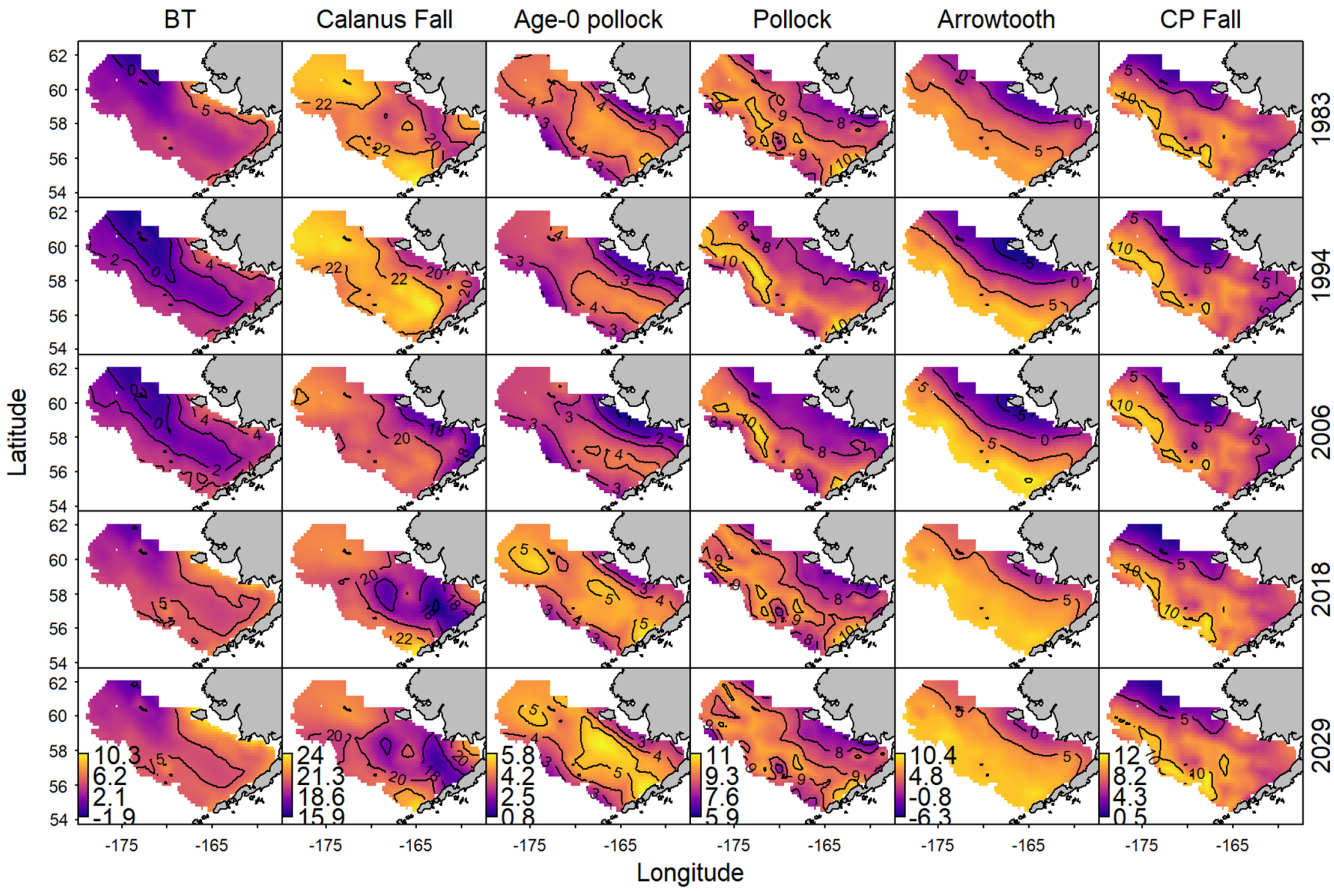

Figure 5. Illustration of estimates for selected variables (columns) in evenly spaced years (rows), showing from left to right column: bottom temperature, fall copepod (*Calanus glacialis* and *C. marshallae* C3-adult) numbers, fall age-0 pollock biomass, summer demersal pollock, summer demersal arrowtooth flounder, B-season fishing effort; bottom row visualizes variables given projected physical conditions in 2029.

all replicates. This high precision is consistent with the tight confidence intervals from the original fit (e.g. comparing black lines in Fig. 7 with intervals in Fig. 4). However, this experiment does not explore the potential impact of model mis-specification upon estimation performance, and this is a useful topic for future research.

Discussion

We have shown how to identify modes of ecosystem variability resulting in community reassembly, as measured by a common overlap metric and forecasted using earth systems models that are driven by global climate projections. To do so, we fitted > 150 000 records spanning four trophic levels (primary, secondary producers, juvenile and adult consumers), as well as ecosystem services regarding human exploitation and migratory species dynamics. The model identifies the spatial niche for each system variable as well as two modes of ecosystem variability, where the dominant index is highly correlated with the spatial extent of cold near-bottom waters. By estimating variable-specific spatial responses to these modes of ecosystem variability, the model identifies that age-0 pollock has decreased spatial overlap with copepods and increased overlap with adult pollock during warm regional conditions, and also that adult pollock have increased overlap with arrowtooth flounder and decreased overlap with catcher–processor fishing effort during these warm years. Given that warm conditions are projected to persist over the coming decade, the model forecasts increased predator–prey overlap involving adult pollock (between age-0 pollock, adult pollock and arrowtooth flounder) and decreased overlap with the copepod forage base and with the catcher–processor fishery during future warming.

Joint analysis of multiple trophic levels (as done here) can synthesize and integrate results that have been studied previously for individual taxa in isolation. For example, Stevenson and Lauth (2019) document northward shifts for gadids and flatfishes during recent warming (including pollock, cod and arrowtooth flounder as illustrated here), and Duffy-Anderson et al. (2017) documented synchronous northward shifts of elevated spring chlorophyll and juvenile (age-0) pollock concentrations. Similarly, Suryan et al. (2016) and others have documented environmental associations and interannual variability for seabirds, and Spencer et al. (2016) forecasted the management implications of changing overlap

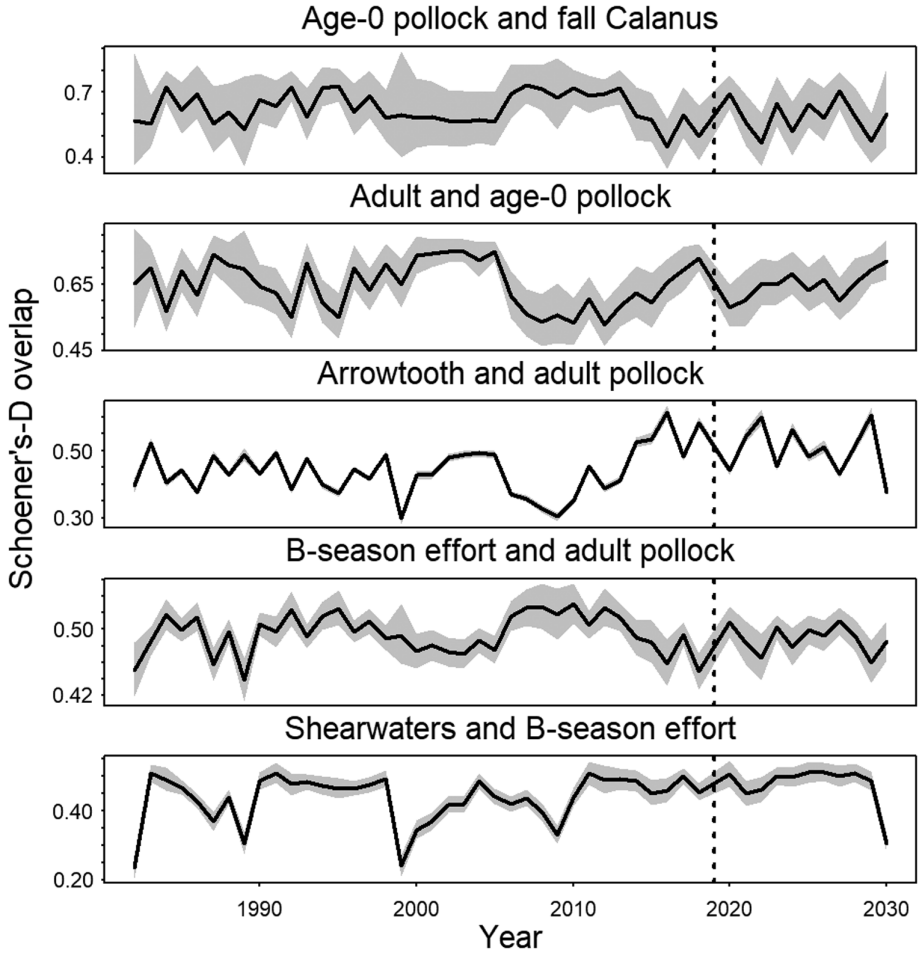

Figure 6. Estimates of Schoener's-D index of overlap between fall surface age-0 pollock and fall vertically integrated copepod densities (top row), summer demersal adult pollock and fall surface age-0 pollock biomass (2nd row), summer demersal pollock and arrowtooth biomass (3rd row), summer demersal pollock and summer/fall midwater fishery effort (4th row), or summer/fall midwater fishery effort and summer/fall shearwater concentrations (line: estimate; shaded area: ± one standard error), while indicating the year (2019) separating physical hindcasts and projections (vertical dotted line). Each panel also indicates the last year of biological data (dotted vertical line), representing the year when the model starts forecasting biological variables based on a projection of ocean physics.

between arrowtooth and adult pollock during future warming. Typically, however, these and other regional analyses for the eastern Bering Sea have not synthesized patterns across multiple trophic levels, and thus did not illustrate climate-driven community reassembly (as we do here). By exploring each variability individually, these past studies for the eastern Bering Sea have been unable, e.g. to identify that warm stanzas are problematic for age-0 pollock (and subsequent recruitment to the fishery at approximately age-3) for two separate reasons: both the decreased overlap with copepods and increased overlap with cannabilistic adult pollock. These and similar insights are only feasible in a joint model for multiple trophic levels and, importantly, the model also provides a formal mechanism to forecast these linkages under future climate conditions (in this case projecting continued obstacles for survival of age-0 pollock). We recommend future studies comparing the jointly estimated mode of variability (as shown here) with the estimated mode of variability for each trophic level and/or ecosystem component individually. This would then identify whether this mode of variability is truly synchronous across all system variables, or results are being highly leveraged by individual model components.

Our model joins the growing list of joint species distribution modelling approaches (Latimer et al. 2009, Hui et al. 2013, Clark et al. 2014, Pollock et al. 2014, Thorson et al. 2015, 2020a, Warton et al. 2015, Ovaskainen et al. 2017a). The preceding studies all estimated covariance (a.k.a. applied ordination) across the occurrence or density of species at a given location. Fewer studies have estimated correlation over time (Thorson et al. 2016, Ovaskainen et al. 2017b, Schliep et al. 2018), and those have typically estimated an autoregressive structure to approximate species interactions (sensu Ives et al. 2003). By contrast, we extend research applying EOF analysis to community ecology (Thorson et al. 2020a), while also using a spatial correlation function to incorporate data following spatially unbalanced designs

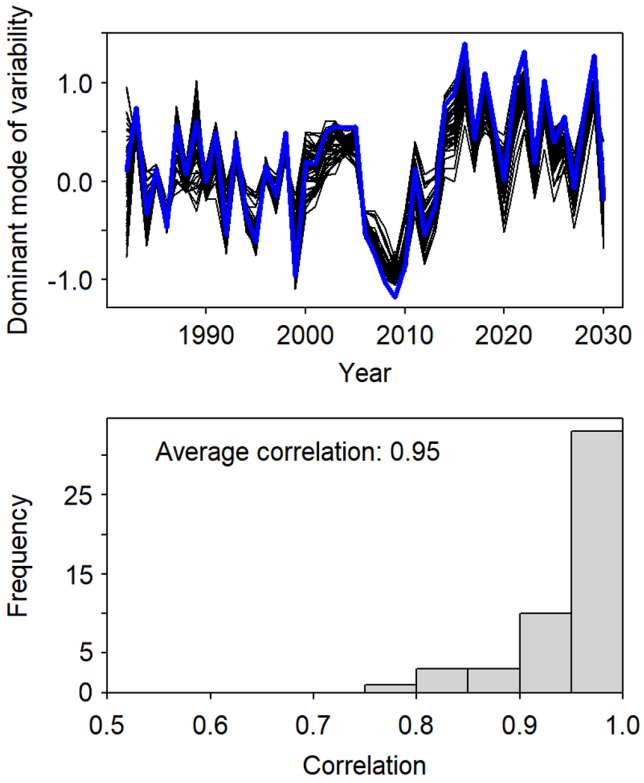

Figure 7. Comparison (top panel) of dominant mode of variability (y-axis) in each year (x-axis) from original fit (blue line) and estimated mode of variability from each of 50 simulation replicates when simulating new data and refitting the model (black lines), as well as the correlation (bottom panel) between original and re-estimated mode of variability in each simulation replicate.

(Thorson et al. 2015, Tikhonov et al. 2020). Applying EOF to community ecology identifies correlations between annual variation in density (within or among species) at any two locations, where these locations can be geographically distant from one another and can be more tightly correlated than locations between the two. Future studies could apply a similar approach to fewer samples (e.g. in ecosystems with less extensive sampling for lower trophic levels), and this could still identify dominant modes of ecosystem variability (Thorson et al. 2020a) albeit without scope to integrate these results across trophic levels.

Wallace and Gutzler (1981) defined teleconnections as 'contemporaneous correlations between geopotential heights on a given pressure surface at widely separated points on earth,' where these nonlocal atmospheric and oceanographic correlations arise due to stochastic but predictable oscillations in physics mechanics. We document a similar occurrence of teleconnections in ecosystem ecology, where the modes of variability estimated here represent correlations between, e.g. spring copepod concentrations in Bristol Bay and summer demersal pollock densities in the northern middle domain. These teleconnections arise in community ecology from physiological and behavioral responses to spatial correlations in regional climate; we hypothesize that these physiological and behavioral mechanisms are nearly as predictable as the causal mechanisms underlying physical teleconnections. Estimating nonlocal associations will be increasingly important when linking joint SDMs to climate variables, e.g. when forecasting future changes in community overlap. In particular, nonlocal dynamics will occur both from migratory and movement behaviors of large-bodied animals, but also from physical advection of nutrients and passive-dispersing juveniles (pollen, plankton and parasites).

Our method identifies shifts in overlap between ecosystem components across five trophic levels. This result provides indirect support for climate-driven shifts in ecosystem interactions, but we recommend further research to incorporate proximal measures of interactions. For example, stomach-content analysis can identify predation between age-0 pollock, demersal pollock and arrowtooth flounder (Livingston et al. 2017), discrete-choice models fitted to fishery catch rates or revenue can identify fishery performance (Haynie et al. 2009), and seabird observers record variability in seabird bycatch (Anderson et al. 2011). Importantly, these analyses are increasingly feasible within a spatio-temporal modelling framework (Grüss et al. 2020), such that physiological and process research can be incorporated into spatial ecosystem models such as this. We therefore recommend further research to fit both distributional data (like those used here) and process data (growth, predation, maturity and reproduction) to improve forecasts of community reassembly. Ideally, this could be done using reanalysis experiments (i.e. withholding recent data when fitting the model, forecasting ecosystem changes and comparing with these recent data) to determine whether forecasted changes in overlap can predict future changes in physiological rates.

Scenario planning under alternative climate futures is an important step towards climate adaptation and resilience (Jurgilevich et al. 2017), and designing effective management requires that models can approximate a wide range of possible scenarios (Punt et al. 2014). Scenario planning is especially important in modeling the effectiveness of climate adaptation and mitigation measures and potential feedbacks with physical, chemical and biological systems (Bonan and Doney 2018). For example, conservation and restoration that benefit multiple stakeholders while addressing climate adaptation and mitigation have received particular attention in climate change literature and assessments (Guerry et al. 2012, Golet et al. 2018). Earth system models capture some elements of potential feedbacks between climate and ecological processes (Bonan and Doney 2018) but often not at the regional scale needed for EBM and conservation planning needs. For this, high resolution ecosystem models as presented herein can inform likely climate trajectories as well as resulting shifts in spatial or temporal reassembly (Theobald et al. 2017, Gouezo et al. 2019). This then allows stakeholders and managers to evaluate unavoidable trade-offs, e.g. between food security and conserving protected species, subsistence and commercial resource use, and current versus future resources.

Data availability statement

Data available from the Dryad Digital Repository: <http://dx.doi.org/10.5061/dryad.b2rbnzsdc> (Thorson et al. 2020b). Data deposited in the Dryad Digital Repository includes all data except catcher-processor fishing effort. These data are confidential and proprietary, and cannot be made available via Dryad. To access these data, please contact A. Haynie (alan.haynie@noaa.gov).

Acknowledgements – We thank the many scientists who have served on the surveys or developed modelling products used here. We also thank G. Hunt, M. Sigler and J. Pearce, and two anonymous reviewers for comments on a previous draft, and R. White for producing the Fig. 1 schematic. Any use of trade, firm or product names is for descriptive purposes only and does not imply endorsement by the U.S. Government.

Author contributions

James Thorson: Conceptualization (lead); Formal analysis (lead); Investigation (lead); Methodology (lead); Project administration (equal); Resources (lead); Software (lead); Supervision (lead); Validation (lead); Visualization (lead); Writing – original draft (lead); Writing – review and editing (equal). **Mayumi Arimitsu**: Data curation (equal); Investigation (equal); Writing – original draft (equal); Writing – review and editing (equal). **Lewis Barnett**: Data curation (equal); Investigation (equal); Writing – original draft (equal); Writing – review and editing (equal). **Wei Cheng**: Data curation (equal); Investigation (equal); Writing – original draft (equal); Writing – review and editing (equal). **Lisa Eisner**: Data curation (equal); Investigation (equal); Writing – original draft (equal); Writing – review and editing (equal). **Alan Haynie**: Data curation (equal); Investigation (equal); Writing – original draft (equal); Writing – review and editing (equal). **Albert Hermann**: Data curation (equal); Investigation (equal); Writing – original draft (equal); Writing – review and editing (equal). **Kirstin Holsman**: Data curation (equal); Investigation (equal); Writing – original draft (equal); Writing – review and editing (equal). **David Kimmel**: Data curation (equal); Investigation (equal); Writing – original draft (equal); Writing – review and editing (equal). **Mike Lomas**: Data curation (equal); Investigation (equal); Writing – original draft (equal); Writing – review and editing (equal). **Jon Richar**: Data curation (equal); Investigation (equal); Writing – original draft (equal); Writing – review and editing (equal). **Elizabeth Siddon**: Data curation (equal); Investigation (equal); Writing – original draft (equal); Writing – review and editing (equal).

References

Alexander, M. A. et al. 2002. The atmospheric bridge: the influence of ENSO teleconnections on air–sea interaction over the global oceans. – J. Clim. 15: 2205–2231.

Anderson, O. R. J. et al. 2011. Global seabird bycatch in longline fisheries. – Endanger. Species Res. 14: 91–106.

Baudron, A. R. et al. 2020. Changing fish distributions challenge the effective management of European fisheries. – Ecography 43: 494–505.

Bonan, G. B. and Doney, S. C. 2018. Climate, ecosystems and planetary futures: the challenge to predict life in Earth system models. – Science 359: eaam8328.

Carroll, G. et al. 2019. A review of methods for quantifying spatial predator–prey overlap. – Global Ecol. Biogeogr. 28: 1561–1577.

Clark, J. S. et al. 2014. More than the sum of the parts: forest climate response from joint species distribution models. – Ecol. Appl. 24: 990–999.

Cressie, N. and Wikle, C. K. 2011. Statistics for spatio-temporal data. – Wiley.

Cressie, N. et al. 2009. Accounting for uncertainty in ecological analysis: the strengths and limitations of hierarchical statistical modeling. – Ecol. Appl. 19: 553–570.

Drew, G. S. and Piatt, J. F. 2015. North pacific pelagic seabird database (NPPSD). – U.S. Geological Survey data release (ver. 3.0, February, 2020), doi: 10.5066/F7WQ01T3.

Duffy-Anderson, J. T. et al. 2017. Return of warm conditions in the southeastern Bering Sea: phytoplankton – fish. – PLoS One 12: e0178955.

Eisner, L. B. et al. 2014. Climate-mediated changes in zooplankton community structure for the eastern Bering Sea. – Deep Sea Res. Part II Top. Stud. Oceanogr. 109: 157–171.

Eisner, L. B. et al. 2016. Late summer/early fall phytoplankton biomass (chlorophyll a) in the eastern Bering Sea: spatial and temporal variations and factors affecting chlorophyll a concentrations. – Deep Sea Res. Part II Top. Stud. Oceanogr. 134: 100–114.

Ettinger, A. and HilleRisLambers, J. 2017. Competition and facilitation may lead to asymmetric range shift dynamics with climate change. – Global Change Biol. 23: 3921–3933.

Farley, E. V. et al. 2007. Juvenile sockeye salmon distribution, size, condition and diet during years with warm and cool spring sea temperatures along the eastern Bering Sea shelf. – J. Fish Biol. 71: 1145–1158.

Golet, G. H. et al. 2018. Using ricelands to provide temporary shorebird habitat during migration. – Ecol. Appl. 28: 409–426.

Gouezo, M. et al. 2019. Drivers of recovery and reassembly of coral reef communities. – Proc. R. Soc. B 286: 20182908.

Gouhier, T. C. et al. 2010. Synchrony and stability of food webs in metacommunities. – Am. Nat. 175: E16–E34.

Grace, J. B. and Irvine, K. M. 2020. Scientist's guide to developing explanatory statistical models using causal analysis principles. – Ecology 101: e02962.

Grüss, A. et al. 2020. Spatio-temporal analyses of marine predator diets from data-rich and data-limited systems. – Fish Fish. 21: 718–739.

Guerry, A. D. et al. 2012. Modeling benefits from nature: using ecosystem services to inform coastal and marine spatial planning. – Int. J. Biodivers. Sci. Ecosyst. Serv. Manage. 8: 107–121.

Hay, L. E. et al. 2000. A comparison of delta change and downscaled GCM scenarios for three mountainous basins in the United States. – JAWRA J. Am. Water Resour. Assoc. 36: 387–397.

Haynie, A. C. et al. 2009. Common property, information and cooperation: commercial fishing in the Bering Sea. – Ecol. Econ. 69: 406–413.

Hermann, A. J. et al. 2019. Projected biophysical conditions of the Bering Sea to 2100 under multiple emission scenarios. – ICES J. Mar. Sci. 76: 1280–1304.
Hollowed, A. B. et al. 2020. Integrated modeling to evaluate climate change impacts on coupled social–ecological systems in Alaska. – Front. Mar. Sci. 6: 775.
Holsman, K. K. et al. 2019. Towards climate resiliency in fisheries management. – ICES J. Mar. Sci. 76: 1368–1378.
Huang, B. et al. 2017. NOAA extended reconstructed sea surface temperature (ERSST), Ver. 5. – NOAA National Cent. Environ. Information, doi:10.7289/V5T72FNM.
Hui, F. K. et al. 2013. To mix or not to mix: comparing the predictive performance of mixture models vs. separate species distribution models. – Ecology 94: 1913–1919.
Ives, A. R. et al. 2003. Estimating community stability and ecological interactions from time-series data. – Ecol. Monogr. 73: 301–330.
Jurgilevich, A. et al. 2017. A systematic review of dynamics in climate risk and vulnerability assessments. – Environ. Res. Lett. 12: 013002.
Kaplan, D. 2001. Structural equation modeling. – In: Smelser, N. J. and Baltes, P. B. (eds), International encyclopedia of the social and behavioral sciences. Pergamon, pp. 15215–15222.
Kass, R. E. and Steffey, D. 1989. Approximate Bayesian inference in conditionally independent hierarchical models (parametric empirical Bayes models). – J. Am. Stat. Assoc. 84: 717–726.
Kimmel, D. G. et al. 2018. Copepod dynamics across warm and cold periods in the eastern Bering Sea: implications for walleye pollock *Gadus chalcogrammus* and the oscillating control hypothesis. – Fish. Oceanogr. 27: 143–158.
Kristensen, K. et al. 2016. TMB: automatic differentiation and Laplace approximation. – J. Stat. Softw. 70: 1–21.
Kuczynski, L. and Grenouillet, G. 2018. Community disassembly under global change: evidence in favor of the stress-dominance hypothesis. – Global Change Biol. 24: 4417–4427.
Latimer, A. M. et al. 2009. Hierarchical models facilitate spatial analysis of large data sets: a case study on invasive plant species in the northeastern United States. – Ecol. Lett. 12: 144–154.
Lauth, R. R. and Conner, J. 2016. Results of the 2013 eastern Bering Sea continental shelf bottom trawl survey of groundfish and invertebrate resources. National Marine Fisheries Service (NMFS) doi: 10.7289/V5/TM-AFSC-331.
Legendre, P. 1993. Spatial autocorrelation: trouble or new paradigm? – Ecology 74: 1659–1673.
Levin, S. A. 1992. The problem of pattern and scale in ecology: the Robert H. MacArthur award lecture. – Ecology 73: 1943–1967.
Lindgren, F. et al. 2011. An explicit link between Gaussian fields and Gaussian Markov random fields: the stochastic partial differential equation approach. – J. R. Stat. Soc. Ser. B Stat. Methodol. 73: 423–498.
Livingston, P. A. et al. 2017. Quantifying food web interactions in the North Pacific – a data-based approach. – Environ. Biol. Fishes 100: 443–470.
Lomas, M. et al. 2020. Time-series of direct primary production and phytoplankton biomass in the southeastern Bering Sea: responses to cold and warm stanzas. – Mar. Ecol. Prog. Ser. 642: 39–54.
Mora, C. et al. 2018. Broad threat to humanity from cumulative climate hazards intensified by greenhouse gas emissions. – Nat. Clim. Change 8: 1062–1071.
Ovaskainen, O. et al. 2017a. How to make more out of community data? A conceptual framework and its implementation as models and software. – Ecol. Lett. 20: 561–576.
Ovaskainen, O. et al. 2017b. How are species interactions structured in species-rich communities? A new method for analysing time-series data. – Proc. R. Soc. B 284: 20170768.
Pinsky, M. L. et al. 2018. Preparing ocean governance for species on the move. – Science 360: 1189–1191.
Pollock, L. J. et al. 2014. Understanding co-occurrence by modelling species simultaneously with a joint species distribution model (JSDM). – Methods Ecol. Evol. 5: 397–406.
Punt, A. E. et al. 2014. Fisheries management under climate and environmental uncertainty: control rules and performance simulation. – ICES J. Mar. Sci. 71: 2208–2220.
Schaefer, H.-C. et al. 2008. Impact of climate change on migratory birds: community reassembly versus adaptation. – Global Ecol. Biogeogr. 17: 38–49.
Schliep, E. M. et al. 2018. Joint species distribution modelling for spatio-temporal occurrence and ordinal abundance data. – Global Ecol. Biogeogr. 27: 142–155.
Schoener, T. W. 1970. Nonsynchronous spatial overlap of lizards in patchy habitats. – Ecology 51: 408–418.
Sigler, M. F. et al. 2016. Variation in annual production of copepods, euphausiids and juvenile walleye pollock in the southeastern Bering Sea. – Deep Sea Res. Part II Top. Stud. Oceanogr. 134: 223–234.
Spencer, P. D. et al. 2016. Modelling spatially dependent predation mortality of eastern Bering Sea walleye pollock, and its implications for stock dynamics under future climate scenarios. – ICES J. Mar. Sci. 73: 1330–1342.
Stevenson, D. E. and Lauth, R. R. 2019. Bottom trawl surveys in the northern Bering Sea indicate recent shifts in the distribution of marine species. – Polar Biol. 42: 407–421.
Suryan, R. M. et al. 2016. Temporal shifts in seabird populations and spatial coherence with prey in the southeastern Bering Sea. – Mar. Ecol. Prog. Ser. 549: 199–215.
Theobald, E. J. et al. 2017. Climate drives phenological reassembly of a mountain wildflower meadow community. – Ecology 98: 2799–2812.
Thorson, J. T. 2018. Three problems with the conventional delta-model for biomass sampling data, and a computationally efficient alternative. – Can. J. Fish. Aquat. Sci. 75: 1369–1382.
Thorson, J. T. 2019. Guidance for decisions using the vector autoregressive spatio-temporal (VAST) package in stock, ecosystem, habitat and climate assessments. – Fish. Res. 210: 143–161.
Thorson, J. T. and Barnett, L. A. K. 2017. Comparing estimates of abundance trends and distribution shifts using single- and multispecies models of fishes and biogenic habitat. – ICES J. Mar. Sci. 74: 1311–1321.
Thorson, J. T. et al. 2015. Spatial factor analysis: a new tool for estimating joint species distributions and correlations in species range. – Methods Ecol. Evol. 6: 627–637.
Thorson, J. T. et al. 2016. Joint dynamic species distribution models: a tool for community ordination and spatio-temporal monitoring. – Global Ecol. Biogeogr. 25: 1144–1158.
Thorson, J. T. et al. 2019. Spatio-temporal models of intermediate complexity for ecosystem assessments: a new tool for spatial fisheries management. – Fish Fish. 20: 1083–1099.
Thorson, J. T. et al. 2020a. Defining indices of ecosystem variability using biological samples of fish communities: a generalization of empirical orthogonal functions. – Prog. Oceanogr. 181: 102244.
Thorson, J. T. et al. 2020b. Data from: Forecasting community reassembly using climate-linked spatio-temporal ecosystem models.

– Dryad Digital Repository, <http://dx.doi.org/10.5061/dryad.b2rbnzsdc>.
Tikhonov, G. et al. 2020. Computationally efficient joint species distribution modeling of big spatial data. – Ecology 101: e02929.
Trenberth, K. E. et al. 2014. Seasonal aspects of the recent pause in surface warming. – Nat. Clim. Change 4: 911–916.
Wallace, J. M. and Gutzler, D. S. 1981. Teleconnections in the geopotential height field during the Northern Hemisphere winter. – Mon. Weather Rev. 109: 784–812.
Walter, J. A. et al. 2017. The geography of spatial synchrony. – Ecol. Lett. 20: 801–814.
Warton, D. I. et al. 2015. So many variables: joint modeling in community ecology. – Trends Ecol. Evol. 30: 766–779.